International Journal of Modern Physics E
Vol. 24, No. 3 (2015) 1530003 (24 pages)

DOI: 10.1142/S0218301315300039

World Scientific
www.worldscientific.com

Modern studies of the Deuteron: From the lab frame to the light front

Werner Boeglin and Misak Sargsian*

Department of Physics,
Florida International University,
Miami, Florida 33199, USA
**sargsian@fiu.edu*

Received 22 January 2015
Accepted 30 January 2015
Published 13 March 2015

We review the recent progress made in studies of deuteron structure at small internucleon distances. This progress is largely facilitated by the new generation of experiments in deuteron electrodisintegration carried out at unprecedentedly high momentum transfer. The theoretical analysis of these data confirms the onset of the high energy eikonal regime in the scattering process which allows one to separate long-range nuclear effects from the effects genuinely related to the short distance structure of the deuteron. Our conclusion is that for the first time the deuteron is probed at relative momenta beyond 300 MeV/c without dominating long-range effects. As a result, at these large nucleon momenta the cross-section is sensitive to the nuclear dynamics at subfermi distances. Due to large internal momenta involved we are dealing with the relativistic bound state that is best described by the light-cone momentum distribution of nucleons in the deuteron. We present the first attempt of extracting the deuteron light-cone momentum distribution function from data and discuss the importance of this quantity for studies of quantum chromodynamics (QCD) structure of the bound nucleon in deep inelastic scattering (DIS) off the deuteron. We conclude the review giving an outlook of the next generation of high energy experiments which will extend our reach to much smaller distances in the deuteron.

Keywords: Deuteron; Electro-Nuclear reactions; nuclear forces; Eikonal.

PACS Number(s): 21.45.Bc, 25.30.−c, 27.10.+h, 11.80.Fv

1. Introduction

The deuteron, discovered in 1931 by Harold Urey (see e.g., Ref. 1), was a theoretical puzzle until the discovery of the neutron in 1932. Since then it has been one of the best 'laboratories' for testing our understanding of the nuclear forces. The evolution of our view of the deuteron was intimately related to the advances in our understanding of the dynamics of the strong interaction.

*Corresponding author.

As an apparent proton–neutron (pn) bound state the deuteron was initially used to explore the large distance phenomena of the pn interaction, which are sensitive to rather general properties of the nuclear force such as its interaction range and the scattering length.

However after the discovery of the deuteron's quadrupole moment, it was clear that the deuteron's structure reflects more intricate properties of the nuclear force such as the tensor interaction. The discovery of pions indicated that the deuteron in addition to proton and neutron may contain also explicit pionic degrees of freedom and indeed pion exchanges between proton and neutron were soon discovered in electromagnetic reactions involving deuteron.[2,3]

Furthermore, the discovery of a rich spectrum of baryonic resonances (R) implied also, in addition to the pn component, the possibility for the existence of NR and RR components in the deuteron (see e.g., Ref. 4). Even richer structures have been predicted with the advent of quantum chromodynamics (QCD) as a fundamental theory of strong interactions. One of the interesting QCD predictions involving the deuteron is the possibility of observing quark–gluon currents in high energy and momentum transfer (hard) reactions involving the deuteron. Such a possibility is identified by a specific energy dependence of the cross-section of the hard reaction (referred as quark counting rule) as well as by polarization observables following from the helicity conservation in quark–gluon interactions.[5] Another unique QCD prediction is the possibility of hidden color states in the deuteron comprising of two color-octet baryons resulting in a colorless deuteron.[6,7]

All above mentioned resonating and QCD properties however reside, kinematically, beyond the NN inelastic threshold which corresponds to deuteron internal momenta above $\sim$370 MeV/c. Thus, this requires an ability of probing significantly shorter distances in the deuteron in which case the overlap of the constituent proton and neutron can be substantial so that one can expect the onset of the quark degrees of the freedom in the NN system.

The understanding of the short-range properties of the deuteron has important relevance to the short-range dynamics of nuclei and nuclear matter with recent observations of the dominance of pn short-range correlations in nuclei,[8] their role in a momentum sharing in asymmetric nuclei[9,10] as well as a possible p^{-4} scaling of the high momentum distribution of nucleons in nuclei.[11]

This paper addresses the present status of the research of short-range properties of the deuteron and expected advances in such studies at new high energy facilities.

The most direct way of probing the short distance structure of the deuteron, is to probe large internal momenta in which case due to the large virtuality of the intermediate states the deuteron wave function is defined by short distance dynamics.

There are several reactions which are expected to probe large internal momenta in the deuteron, such as elastic $ed \to ed$ processes at high momentum transfer (for a review see Ref. 12), or inclusive $ed \to e'X$ processes in the quasielastic region at the so-called large $-y$ region (for review see Ref. 13). These reactions have larger

cross sections and historically they were the first aimed at probing short-range properties of the deuteron. However due to the specifics of these reactions only integrated properties of the deuteron momentum distribution are accessed. As a result the ability of using these reactions to probe the deuteron at extremely large internal momenta is rather restricted.

The most direct way of probing the internal structure of the deuteron is to study the exclusive

$$e + d \to e' + p + n, \tag{1}$$

reaction in which one of the nucleons is struck by the incoming electron and the other is a spectator to the reaction.

First, such exclusive experiments were attempted in the early 60's using electron probes of a few 100 MeV. Due to the very small duty factor of these early accelerators and the extremely small cross-section of the coincidence reaction only measurements at small nucleon momenta were possible.[14,15]

Starting in the 70s, when the duty factor of electron accelerators increased, attempts to probe larger nucleon momenta were carried out providing first cross-section data for nucleon momenta up to 300 MeV/c[16,17] and in the 80s cross-section measurements at internal nucleon momenta beyond 300 MeV/c were carried out at Saclay.[18,19] The theoretical analysis of these data established that due to the lack of resolving power of the probe ($Q^2 \ll M_N^2$ GeV^2) the cross-section of the reaction (1) at internal relative pn momenta $\geq$ 300 MeV/c was dominated by long-range processes such as final state interaction (FSI), intermediate isobar contributions as well as meson exchange currents (MEC).

The situation changed only after the appearance of the high energy and high duty cycle continuous electron beam accelerator facility (CEBAF) accelerator, where it was, for the first time, possible to perform dedicated large momentum transfer ($Q^2 > M_N^2$ GeV^2) experiments of the reaction (1).

In this paper, we review the chronology of the experimental studies of exclusive electro-disintegration of the deuteron (1) and elaborate how the increase of the transferred momentum made it possible to access and probe the smaller internal distances in the deuteron. We demonstrate the qualitative changes that high momentum transfer processes bring into the observables and the emergence of the new theoretical approximation in describing the reaction (1) in the high energy limit.

One of the main changes in the high energy limit is the emergence of the light-front dynamics in probing the relativistic internal structure of the deuteron and the possibility of extracting the light-cone momentum distribution of the bound nucleon in the deuteron. We present the first such extraction using the recent high momentum transfer data from Jefferson Lab (JLab).

We conclude the paper demonstrating how the eikonal regime allows an extension of the deuteron studies to internal momenta in and above the GeV region. Such momenta can be experimentally studied at JLab after the 12 GeV energy upgrade.

2. The Modern View of the Deuteron

We start with decomposing the deuteron state vector into the Fock states restricted by the total spin, $S = 1$ and isospin, $T = 0$ quantum numbers of the deuteron:

$$\Psi_d = \Psi_{pn} + \Psi_{\Delta\Delta} + \Psi_{NN^*} + \Psi_{hc} + \Psi_{NN\pi} \cdots, \tag{2}$$

the "$\cdots$"'s include the contributions from higher Fock components and higher mass constituents. In the following, we will discuss separately each component presented in Eq. (2).

2.1. *pn component*

Kinematically one expects pionic degrees of freedom to become relevant at deuteron internal momenta exceeding $\frac{\sqrt{s_{\rm thr}-4m_N^2}}{2} \approx 370\,{\rm MeV}/c$. However the empirical evidence suggests that the pn component is dominant for deuteron internal momenta up to $650\,{\rm MeV}/c$ (see e.g., discussion in Ref. 20). This can be understood based on the following facts: (i) the proportionality of the $N\pi N$ vertex to the pion momentum, (ii) the form factor of $N \to \pi N$ transition being hard $\sim \exp \lambda t$ with $\lambda \geq 3\,{\rm GeV}^{-2}$ (see Ref. 21) and (iii) the processes in which the high energy probe couples to the exchanged pion in the deuteron is significantly suppressed at high momentum transfer. These facts indicate that the dominant inelastic component can be the $\Delta\Delta$ rather than the $N\pi N$ component which will extend the pn dominance for up to $p \sim 800\,{\rm MeV}/c$. Despite the possibility for such a dominance, the pn component of the deuteron wave function currently is reliably understood only for up to $400\,{\rm MeV}/c$. Many factors contribute to this uncertainty such as the insensitivity of the small distance phenomena to the accuracy of the NN phase shifts, relativistic effects and the treatment of the pion threshold in the NN channel.

2.2. $\Delta\Delta$ *component*

Due to the large cross-section of the $\pi N \to \Delta$ transition and the above discussed suppression of the $N\pi N$ transition one expects the largest nonnucleonic component in the deuteron to be the $\Delta\Delta$ component. The current experimental constraints on the overall contribution of the $\Delta\Delta$ component is $\leq 1\%$.

2.3. NN^* *component*

In principle, the quantum numbers of the deuteron allow the NN^* component which will correspond to the radial excitation of one of the nucleons in the deuteron. Such an excitation will require an energy of $\sim$600 MeV/c corresponding to internal momenta similar to the $\Delta\Delta$ component ($\sim$800 MeV/c). However, empirically one expects a smaller $NN \to NN^*$ amplitude which may result in a contribution smaller than the contribution from the $\Delta\Delta$ component. Currently there is no experimental evidence or constraint on the possible mixture of the NN^* component.

2.4. *Hidden color component*

One of the unique predictions of QCD is the existence of the hidden color component in the deuteron wave function. In fact the color decomposition of a six-quark (6q) system predicts almost 80% of the wave function strength to be due to the hidden color component.[6,7] However, one expects such a dominance only to occur at very large excitation energies of the NN system when the sum of the possible two-baryonic states in the deuteron is replaced by the six-quark representation. Since such large excitation energies are relevant to the nuclear core, it rises an interesting possibility of the NN repulsive core being the result of the suppressed overlap between a hidden color dominated configurations and the NN component.

2.5. *$NN\pi$ component*

Finally, the most dominant three-particle Fock component of the deuteron is the $NN\pi$ component which one may expect to appear at excitation energies close to the pion threshold (corresponding to an internal momentum of $\sim$370 MeV/c) and to be sensitive to the external probe at low momentum transfer. There is plenty of evidence of this component from low and intermediate energy reactions which probed MEC that start to dominate at the missing momentum range of $\sim$350 MeV/c consistent with the above estimate of the pion threshold (see for example Refs. 2 and 3).

3. Basic Diagrams and Kinematic Definitions of the Exclusive Reaction

For definiteness, we assume that the detected particles at the final state of the reaction (1) are the scattered electron and proton while the neutron is reconstructed through the energy–momentum conservation. We define the transferred four-momentum as $(q_0, \mathbf{q})$ with a virtuality of $Q^2 = \mathbf{q}^2 - q_0^2$ and $(E_p, \mathbf{p_p})$ and $(E_n, \mathbf{p_n})$ as the four-momenta of the final proton and neutron respectively. We also define the missing momentum, p_m,

$$-\mathbf{p_m} \equiv \mathbf{p_i} = \mathbf{p_p} - \mathbf{q} = -\mathbf{p_n}, \tag{3}$$

which in the special case (see below) can be interpreted as a negative initial momentum vector of the bound proton which interacts with the electron.

Within the one-photon exchange approximation the basic Feynman diagrams that describe the exclusive process of Eq. (1) are given in Fig. 1.

These diagrams can be categorized as follows:

(i) Direct plane-wave impulse approximation (PWIA) contribution: We call the contribution of Fig. 1(a) a direct PWIA term, in which the detected nucleon (proton in the example) is knocked-out by the virtual photon while the undetected nucleon (neutron) is a spectator to the $\gamma^* p_{\rm bound} \to p_{\rm final}$ scattering. No FSI is considered and therefore final nucleons emerge as plane waves.

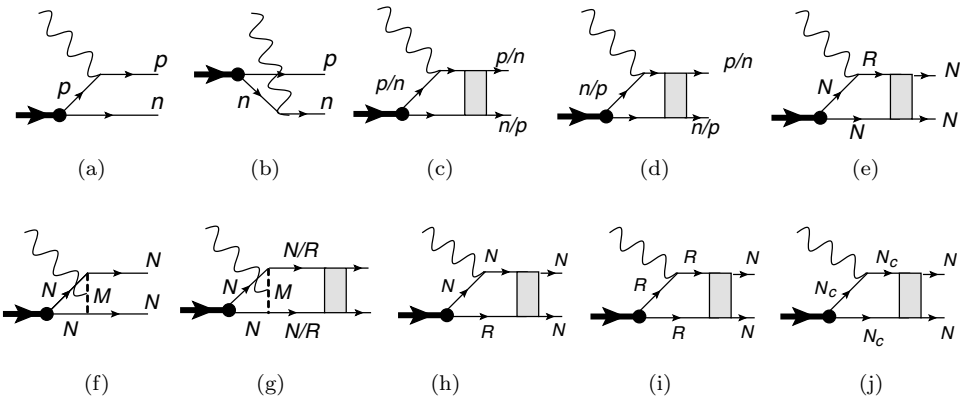

Fig. 1. Diagrams contributing to the exclusive $d(e, e'p)n$ reaction.

(ii) Spectator PWIA contribution: In Fig. 1(b), it is the undetected neutron which is struck by the virtual photon while the detected proton emerges as a spectator. Again no FSI is considered between the emerging nucleons.

(iii) Direct FSI contribution: In this case (Fig. 1(c)), the struck proton rescatters off the spectator neutron and is detected in the final state.

(iv) Charge-interchange FSI contribution: In this case (Fig. 1(d)), the struck nucleon undergoes a charge interchange interaction with the spectator nucleon.

(v) Intermediate state resonance production: In Fig. 1(e), the electromagnetic interaction excites the nucleon into a resonance state which then rescatters with the spectator nucleon into the final proton and neutron.

(vi) Meson exchange contributions: In Figs. 1(f) and 1(g), the electromagnetic interaction takes places with the mesons which are exchanged between initial nucleons in the deuteron.

(vii) Nonnucleonic contributions: Final three terms contributing to the reaction (Figs. 1(h)–1(j)) are sensitive to the nonnucleonic component of the deuteron wave function. Here the first two represent the baryonic and the last, the hidden color component contributions which was discussed in the Sec. 2.

4. Concept of Probing the High Momentum Component of the Deuteron

To probe the high momentum NN component of the deuteron, in the diagrammatic presentation of the scattering process of Eq. (1), is to isolate the contribution from the direct PWIA process[a] (Fig. 1(a)) at such momentum transfer $\mathbf{q}$ and final proton momentum $\mathbf{p_p}$ that the calculated missing momentum, according to Eq. (3), $p_m > 300\,\mathrm{MeV}/c$.

[a]Hereafter refereed as PWIA process.

Such an isolation however requires a suppression or reliable accounting for all the remaining contributions (diagrams Figs. 1(b)–1(j)) discussed in the previous section.

Our assertion is that this can be achieved if we consider the reaction (1) in *high energy* kinematics in which the transferred momentum $q \geq$ few GeV/c and the virtuality of the probe, $Q^2 > 1\,\mathrm{GeV}^2$, with an additional condition that the final nucleons (proton in our case) carries almost all the momentum of the virtual photon while the recoiling nucleon (neutron) is significantly less energetic, i.e.,

$$\begin{aligned} & p_p \sim q \sim \text{few GeV/c}, \\ & |p_n| = |\mathbf{q} - \mathbf{p}_p| \sim \text{few hundred MeV}/c \quad \text{and} \quad Q^2 > 1\mathrm{GeV}^2. \end{aligned} \tag{4}$$

The effects of the above conditions are different for different diagrams of Figs. 1(b)–1(j), which we can categorize as *kinematical*, *dynamical* and the mixture of both.

The suppression of the spectator PWIA diagram, Fig. 1(b), is purely *kinematical*, since in this case the amplitude of the scattering will be defined by the deuteron wave function, $\sim\psi_d(p_p)$ with the initial momentum of $p_p \sim$ few GeV/c as compared to the PWIA term which is proportional to $\sim\psi_d(p_n)$ with $p_n \sim$ few hundred MeV/c.

The diagrams containing MEC (Figs. 1(f) and 1(g)) will be suppressed *dynamically*, since in the limit of $Q^2 \gg m^2_{\mathrm{meson}} \sim 1\,\mathrm{GeV}^2$ they are suppressed compared to the PWIA term by an extra factor of Q^6.[22,23] Another dynamical suppression occurs in the scattering followed by the charge-interchange rescattering (Fig. 1(d)). In this case the suppression is due to an extra $s^{-1/2}$ factor as well as a much stronger t dependence in the $pn \to np$ amplitude as compared to the $pn \to pn$ amplitude that enters in the direct FSI contribution (Fig. 1(c)).[24] The same is true for processes involving nonnucleonic components of the deuteron wave function (Figs. 1(h)–1(j)), since in this case rescattering amplitudes are nonpomeron exchange type decreasing with s as compared to the almost s-independent $pn \to pn$ amplitude. Additionally one expects negligible contributions due to nonnucleonic components for deuteron internal momenta up to 700–750 MeV/c.[20]

Finally, the suppression of processes involving intermediate baryonic resonance production (Fig. 1(e)), which is expected to be large in the $\gamma N \to \Delta$ channel, is due to both kinematical and dynamical reasons. Kinematically, in the high energy limit it is possible to probe the lower q_0 side of the quasielastic peak (corresponding to Bjorken variable $x_{\mathrm{Bj}} = \frac{Q^2}{2m_N q_0} > 1$) which is maximally away from the inelastic threshold of Δ electroproduction. Dynamically, due to the spin-flip nature of the $\gamma^* N \to \Delta$ transition one expects a much steeper falloff of the transition form factor with Q^2 as compared to the elastic $\gamma^* N \to N$ scattering.[25,26]

The above discussion leaves us with the dominating contributions from the PWIA (Fig. 1(a)) and direct FSI (Fig. 1(c)[b] diagrams only. There is no obvious

[b]Referred hereafter as FSI diagram.

reason for the suppression of the latter diagram, since in the high energy limit the amplitude of $pn \to pn$ rescattering at small angles is dominated by the pomeron exchange and is practically energy independent. However the most important change of the character of FSI in the high energy limit is the onset of the eikonal regime, in which case FSIs exhibit a strong angular anisotropy[c] being large at transverse and small at longitudinal directions of the recoil (slow) nucleon production.

Thus, we expect that in the high energy limit, defined according to Eq. (4), the cross-section of the process (1) will be defined mainly by the PWIA (Fig. 1(a)) and FSI (Fig. 1(c)) processes. In this case, the concept of probing the high momentum component of the deuteron is related to measuring process (1) at large values of p_m which in the lab frame of the deuteron within PWIA corresponds to a large internal momentum in the deuteron. Such large missing momenta should be measured at forward or backward recoil nucleon angles which will minimize FSI effects allowing the direct access to the PWIA term.

5. Previous $d(e, e'p)n$ Experiments and the Impossibility of Probing the Deuteron at Short Distances

Before discussing the recent high energy experiments we briefly review the previous experiments at low and intermediate energies.

Since the beginning of electron scattering experiments in the 1950's it was recognized that coincidence experiments have the potential to provide a new, detailed information on the nuclear wave function.[27] One of the first $d(e, e'p)n$ experiments was performed at the Stanford Mark III accelerator, where the coincidence cross-section was measured for a very low missing momentum[14] at a four-momentum transfer, $Q^2 = 0.085$ $(\mathrm{GeV}/c)^2$. Shortly thereafter the range in missing momenta probed was extended to almost 100 MeV/c by the experiment of Bounin and Croissiaux at the Orsay linear accelerator.[15] The smallest coincidence cross sections accessible in these early experiments were determined by the small duty cycle of the available accelerators (of the order of $1{\cdot}10^{-5}$). For a given average current, a small duty cycle leads to very high instantaneous particle rates and large contributions of accidental coincidences which makes the measurement of small cross-secession very difficult.

Starting in the 1970s a new generation of experiments were performed at intermediate electron beam energies and higher duty factors, further extending the measured range of missing momenta. Experiments carried out at the Kharkov institute with the 2 GeV linear accelerator (duty cycle $\approx 2{\cdot}10^{-4}$) were able to extend the missing momenta probed to 300 MeV/c and found large deviations from the PWIA results for missing momenta above 100 MeV/c.[16,17] These measurements were followed by experiments at Saclay[18,19] in the 1980s that extended the missing

[c]This should be contrasted with the large and almost isotropic FSI at low and intermediate energies.

momentum coverage for the first time to 500 MeV/c using new instrumentation and the Saclay linear accelerator (ALS) with the duty factor of $1 \cdot 10^{-2}$.

The large missing momentum data in these experiments were taken at a quite small momentum transfer. Interestingly, the measured cross sections at large $p_m \sim 350\,\mathrm{MeV}/c$ turned out to be quite close to the PWIA prediction. The calculations[3] including direct and spectator PWIA as well as FSI, MEC and IC demonstrated that at these specific kinematics a cancelation seems to occur between FSI, MEC and IC contributions resulting in a calculated momentum distribution which is in quite good agreement with the PWIA prediction which includes both direct and spectator contributions.

With the advent of new high duty factor (∼1) electron accelerators in the 1990's it became possible to measure very small cross sections with very little accidentals in a comparatively short amount of time. This made it possible to extend the measurement of the $d(e, e'p)n$ cross-section up to missing momenta of 928 MeV/c in a deuteron electro-disintegration experiment at the Mainz Microtron (MAMI).[29,30] However, in order to reach these extreme kinematic settings with the available

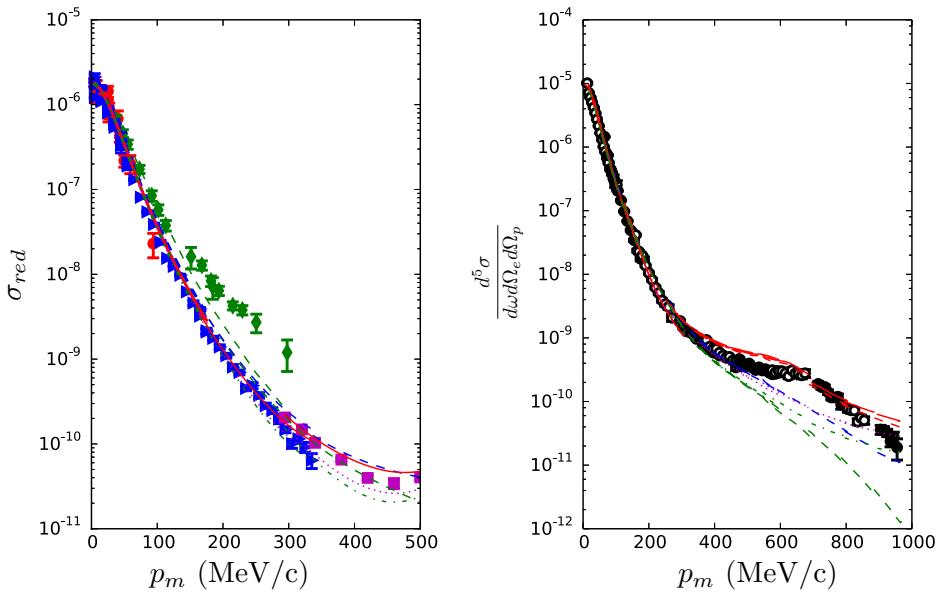

Fig. 2. (Color online) Left: The reduced cross sections as measured at Saclay together with the earlier experiments. The red circles are from Ref. 15, the green diamonds from Ref. 17, the blue triangles from Ref. 18 and the magenta squares from Ref. 19. The lines are calculations by Arenhövel.[28] The green dashed line is a PWIA calculation, the blue dashed line corresponds to PWIA, the green dash–dotted line includes FSI, the dotted magenta line includes FSI+MEC, the solid red line includes FSI+MEC+IC (IC: Intermediate Δ resonance contribution) and the dashed red line includes FSI+MEC+IC+R (R: relativistic corrections); Right: The cross sections measured in the Mainz experiment[29] compared to calculations by Arenhövel. The labeling of the curves in the two panels is identical.

electron beam energy and detection capabilities, virtually no room was left to select the kinematics in such a way as to minimize FSI, MEC and IC contributions. Indeed, it was found that the cross sections at high missing momenta were dominated by long-range processes such as FSI, MEC and IC contributions. The comparison with the theory demonstrated that for missing momenta above $\approx 300\,\mathrm{MeV}/c$ the large FSI, MEC and IC contributions do not mutually cancel and completely obscure the short-range PWIA contribution (Fig. 2).

The dominance of IC and MEC contributions were understood based on the fact that at $\geq 300\,\mathrm{MeV}/c$ one is very close to the inelastic threshold in which the scattering proceeds through the copious pion and isobar production in the intermediate state of the reaction. The large and isotropic FSI is due to the fact that at moderate momentum transfer q, the struck and recoil nucleons in the final state have small and comparable momenta at $p_m \geq 300\,\mathrm{MeV}/c$. Consequently the rescattering is taking place at small relative momenta at which two nucleons are in the relative S-state and have a large interaction cross section. The dominance of the relative S-state leads to the observed isotropic distribution of the FSI strength.

6. First High Q^2 $d(e, e'p)n$ Experiments

With the availability of the CEBAF at JLab, new experiments became possible with a beam energy of up to 6 GeV, a duty factor of one and a total beam current of up to 200μ A. This machine, unique in the world, allowed one for the first time to study the $d(e, e'p)n$ reaction at both high $Q^2(\geq 1)\,\mathrm{GeV}^2$ and high missing momenta.

6.1. *Experiments*

Two recent JLab $d(e, e'p)n$ experiments, using the CEBAF large acceptance spectrometer (CLAS) in Hall B and the two high resolution spectrometers (HRS) in Hall A, measured the $d(e, e'p)n$ cross sections for large missing momenta, p_m up to $550\,\mathrm{MeV}/c$ at various Q^2 ($> 1\,\mathrm{GeV}^2$) and neutron recoil angles, θ_{nq} (the angle between the recoiling neutron and the three-momentum transfer $\mathbf{q}$). The CLAS experiment[31] took advantage of the large acceptance of its detector making it possible to measure a wide range of kinematic settings simultaneously. The $d(e, e'p)n$ cross section was measured for a range of four-momentum transfers $1.75 < Q^2 < 5.5\ (\mathrm{GeV}/c)^2$, for each Q^2 setting centered around $Q^2 = 2 \pm 0.25, 3 \pm 0.5, 4 \pm 0.5, 5 \pm 0.5\,\mathrm{GeV}^2$. The cross sections were measured as a function of θ_{nq} for three ranges of missing momenta: (i) $p_m < 100$ MeV/c; (ii) $200\,\mathrm{MeV}/c < p_m < 300\,\mathrm{MeV}/c$ and (iii) $400\,\mathrm{Mev}/c < p_m < 600$. In addition, the extracted cross sections were integrated over the range of azimuthal angles, ϕ (the angle between the electron scattering plane, (eq) and the reaction plane defined by the momentum transfer vector and the momentum vector of the ejected proton, (qp_p)) covered by the CLAS acceptance. This experiment provided a very nice overview of the general behavior of the $d(e, e'p)n$ cross-section over a wide kinematic range.

In the Hall A experiment, the two HRS were used to measure the neutron recoil angle, θ_{nq}, dependence of the $d(e,e'p)n$ cross sections for fixed sets of Q^2 and missing momenta, p_m. In contrast to the CLAS experiment, in the Hall A experiment the kinematic range probed by each spectrometer setting was much narrower. This allowed the determination of a consistently averaged kinematics for each measured points. This in turn simplifies the comparison of the experimental data with theoretical calculations as there is no need to perform a full Monte Carlo calculations to include the acceptance effects into the theory prediction. In the Hall A experiment the kinematic settings were optimized to measure angular distributions for the missing momenta $p_m = 200 \pm 20{,}400 \pm 20{,}500 \pm 20\,\mathrm{MeV}/c$. The largest measured value of θ_{nq} was determined by the largest proton momentum accessible to the proton spectrometer. Angular distributions were extracted for the four-momentum transfers $Q^2 = 0.8 \pm 0.25, 2.1 \pm 0.25, 3.5 \pm 0.25\,\mathrm{GeV}^2$. First results obtained at the highest four-momentum transfer $Q^2 = 3.5\,(\mathrm{GeV}/c)^2$ have been published.[32]

6.2. *Data*

The CLAS/Hall B experiment measured the recoil neutron's angular and momentum dependences of the cross-section in which the data were integrated over the large intervals of neutron momenta (for the θ_{nq} dependence) and the whole range of recoil angles for the p_n dependence. The theoretical comparison with the data required an identical integration of the theoretical cross-section over the acceptance of CLAS detector.

The Hall A data too measured the recoil neutron's angular and momentum dependences but for significantly smaller kinematical bins. As a result the theoretical predictions could be directly compared with the data. For the angular dependence the data were presented in the form of the ratio:

$$R = \frac{\sigma^{\mathrm{exp}}}{\sigma^{\mathrm{PWIA}}}, \tag{5}$$

where σ^{exp} represents the differential cross-section, $\frac{d\sigma}{dE'_e d\Omega_e d\Omega_n}$, and σ^{PWIA} is the same differential cross section calculated within PWIA. The reason of considering such a ratio was that in the high energy limit it should approach unity for diminishing FSI contribution. Thus the ratio, R, is most appropriate for studying FSI effect in the $ed \to e'pn$ reaction.

For studying the momentum distribution, the Hall A data were presented in the form of the reduced cross sections, defined as

$$\sigma_{\mathrm{red}} = \frac{\sigma^{\mathrm{exp}}}{K\sigma_{ep}}, \tag{6}$$

where σ_{ep} is the theoretical cross-section of the electron scattering off the bound proton with momentum p_i, in which the cofactor, K, is fixed in such a way that in the PWIA limit σ_{red} gives the deuteron momentum distribution $n_d(p_i)$.

It is worth mentioning that theoretical calculations of $\sigma^{\rm PWIA}$ (in Eq. (5)) and σ_{ep} (in Eq. (6)) contain uncertainties due to relativistic effects and off-shellness of the bound proton which increase with increasing neutron recoil momentum. Therefore, the precise theoretical analysis will require a careful account of these effects.

As will be discussed in Sec. 7 the angular distributions of both experiments clearly exhibit the onset of the eikonal regime for the FSI processes. The momentum distributions however differ in these experiments. The CLAS data for the given missing momentum bin have been integrated over the whole range of the recoil nucleon's angle. As a result the momentum distributions do not separate regions in which FSI contributions are minimal to allow the extraction of the experimental deuteron momentum distribution at large missing momenta.

On the other hand, the much smaller kinematic bin sizes in the Hall A data enabled the extraction of momentum distributions for fixed recoil angles with well-defined kinematic settings for each p_m bin. As a result the dependence of the reduced cross-section is studied as a function of the recoil neutron angle and thus for various degrees of FSI contributions. As will be shown in Sec. 8, by selecting a θ_{nq} region in which FSI is minimal one can measure the $d(e,e'p)n$ cross sections being dominated by the short-range structure of the deuteron.

7. Window to Short Distances in the Deuteron at Large Momentum Transfer Processes

As mentioned previously with increasing momentum and energy transfers, the eikonal regime is expected to be established. This leads to a strong angular anisotropy of FSI, with the pn reinteraction dominating at kinematics in which the recoiling nucleon is produced at almost transverse angles with respect to the transfered momentum q.

However, the most important feature of the eikonal regime of rescatterings is that it creates a unique possibility for the cancelation of FSIs at large values of missing (or recoil) momenta. To see this we present the $ed \to epn$ scattering amplitude within the generalized eikonal approximation (GEA)[22,24,33]:

$$\begin{aligned} A^{\mu} = A_0^{\mu} + A_1^{\mu} = & \sqrt{2(2\pi)^3 2E_r}\Psi_d(p_i) j_N^{\mu}(p_i+q,p_i) \\ & - \frac{\sqrt{2(2\pi)^3}}{2}\int \frac{d^3p_i'}{(2\pi)^3}\frac{\sqrt{2E_r'}\sqrt{s(s-4m_N^2)}}{2E_r'q} \\ & \times \frac{f_{pn}(p_i'-p_i)}{p_{i,z}+\Delta-p_{i,z}'+i\varepsilon} j_N^{\mu}(p_i'+q,p_i')\psi_d(p_i'), \end{aligned} \tag{7}$$

where $p_r \equiv p_n$ is the recoil nucleon momentum and $\mathbf{p}_i = -\mathbf{p}_r$ is the initial momentum of the struck nucleon within PWIA. The initial momentum of the struck nucleon in the FSI amplitude is defined as $p_i' \neq -\mathbf{p}_r$. In the high energy limit the factor, $\Delta \approx \frac{q_0}{\mathbf{q}}(E_r - m_N)$, where E_r is the energy of the recoil nucleon. Also $s = (q+p_d)^2$ is the total invariant energy of the reaction.

The Eq. (7) allows one to make several general conclusions about the structure of FSI in the high energy limit.

7.1. *First - kinematical constraints*

The existence of the pole in the rescattering amplitude of Eq. (7) indicates that the rescattering defines the initial longitudinal momentum of the struck nucleon at,

$$p'_{i,z} = p_{i,z} + \Delta. \tag{8}$$

Because both Δ and $p_{i,z} = -p_{r,z}$ are defined by the external kinematics of the reaction, one can have a way of controlling the magnitude of the initial nucleon momentum before the rescattering thus suppressing FSI as compared to the PWIA amplitude. For example if one satisfies the condition:

$$|p'_{i,z}| > |p_{i,z}|, \tag{9}$$

then the rescattering amplitude will be suppressed due to the larger momentum of the deuteron wave function entering in the FSI term as compared to that of the PWIA term. Since Δ is always positive, such a condition is automatically satisfied for positive $p_{i,z}$'s which correspond to the production of the spectator nucleon in backward directions.

One can also estimate the initial transverse momentum of the struck nucleon in the FSI amplitude noticing that in the high energy limit the pn rescattering has a diffractive nature:

$$f_{pn} = \sigma_{\rm tot}(i+\beta)e^{\frac{B_{NN}}{2}t} \approx i\sigma_{\rm tot}e^{-\frac{B_{NN}}{2}k_t^2}, \quad \beta \ll 1, \tag{10}$$

where $\sigma_{\rm tot}$ is the total cross section of pn scattering and B_{NN} is the slope factor of the elastic differential cross-section. Using this and Eq. (7), we notice that the transverse momentum of the initial nucleon is related to the measured transverse momentum $\mathbf{p}_{i,t} = -\mathbf{p}_{r,t}$ as:

$$\mathbf{p}'_{i,t} = \mathbf{p}_{i,t} + \mathbf{k}_t, \tag{11}$$

where $\langle k_t^2 \rangle \sim \frac{2}{B_{NN}}$. This relation indicates that FSI will be maximal at $\mathbf{p}_{i,t} \approx -k_t$ corresponding to smaller $p'_{i,t}$ and minimal at $|\mathbf{p}_{i,t}| \ll |k_t|$ corresponding to $p'_{i,t} \sim k_t$, which enters the deuteron wave function in the FSI amplitude.

The above observations on longitudinal and transverse components of the struck nucleon's initial momenta allow us to predict that the FSI will be small at small p_r and very anisotropic at large p_r: Dominating at transverse ($p_r \perp q$) and being suppressed at parallel/antiparallel ($p_r \| q$) kinematics.

7.2. *Second - cancelation of FSI*

Using the fact that in the high energy limit the pn scattering amplitude is predominantly imaginary (Eq. (10)), one can demonstrate that at large recoil momenta p_r, it is always possible to find kinematics in which the FSI amplitude being large is

cancelled in the cross-section. The reason for such a cancelation is in the fact that the PWIA and imaginary part of the FSI amplitude enter with opposite signs creating an option in which case the PWIA/FSI interference cancels the modulus-square of the FSI amplitude.

To demonstrate this, on a qualitative level, we consider the expression of $|A^\mu|^2$ from Eq. (7), performing the following simplifications which preserve the eikonal nature of the scattering: (i) We use the analytic form of Eq. (10) considering the pn amplitude as purely imaginary, (ii) we neglect by small principal value part of Eq. (7) and factorize the electromagnetic current j^μ from the integrand. After these approximations one obtains from Eq. (7) the following condition for the cancelation of the FSI contribution in the cross-section:

$$\psi_d(p_r) = \frac{1}{8}\int \frac{d^2k_t}{(2\pi)^2}\sigma_{\rm tot}e^{-\frac{B_{NN}}{2}k_t^2-\frac{B_{NN}}{2}\Delta^2}\psi_d(\tilde{p}_r), \tag{12}$$

where $\tilde{p}_r = (p_{r,z}-\Delta, p_{r,t}-k_t)$ is defined by the pole value of the integral in Eq. (7).

We can now solve the above equation analytically if we simplify the deuteron wave function in the form of $\psi_d = Ce^{-\alpha_d p^2}$, in which by using a harmonic-oscilliator (HO) model of the deuteron one relates the α_d parameter to the root-mean-square (rms) radius and momentum of the deuteron: $\alpha_d = \frac{r_{\rm rms}}{2p_{\rm rms}}$. Using this approximation and neglecting the recoil factor Δ one arrives at a very simple analytic relation for the cancelation of the FSI:

$$p_{r,t}^2 = \frac{1}{\alpha_d}\ln\frac{32\pi\alpha_d}{\sigma_{NN}} \approx \frac{1}{\alpha_d}\ln\alpha_d, \tag{13}$$

where in the derivation we also used the relation $\alpha_d \gg B_{NN}$. In the last part of the equation, we used the known value of $\sigma_{pp} = 40$ mb, which results in $\frac{32\pi}{\sigma_{NN}} \approx 1$ GeV^2. For the estimation of α_d according to the HO approximation we use $r^d_{\rm rms} = 2.13\,$fm (see Ref. 36) and $p_{\rm rms} = 135\,{\rm MeV}/c$[d] obtaining $\alpha_d \approx 40\,{\rm GeV}^{-2}$ and

$$|p_{r,t}| \approx 300\,{\rm MeV}/c. \tag{14}$$

This result indicates that there is always a characteristic transverse momentum defined by the properties of the deuteron and the characteristic spatial range of the high energy pn scattering ($\sigma_{pn} \sim r^2_{pn}$) at which the interference between PWIA and FSI amplitudes (screening term) cancels the modulus-square of the FSI amplitude (rescattering term). Such cancelation happens at two angles corresponding to the production of the recoil nucleon in the forward and backward directions, namely:

$$\sin(\theta_{c1}) = \sin\left(\frac{\pi}{2}+\theta_{c2}\right) = \frac{p_{r,t}}{p_r} \sim \frac{300\,{\rm MeV}/c}{p_r}. \tag{15}$$

This simplified estimate shows that starting at $p_r > \sim 300\,{\rm MeV}/c$ at two angles of spectator nucleon production one expects a cancelation of the FSI effects thus opening a window for probing deuteron at large internal momenta.

[d]Which is estimated using the deuteron momentum distribution based on V18 NN potential.[37]

It is worth mentioning that this cancelation is inherent to high energy scattering and is observed in all theoretical calculations based on the eikonal approximation (see e.g. Refs. 22, 24, 33, 34 and 38–48).

The above discussed feature of FSI has been experimentally confirmed in the first high $Q^2(\geq 2\,\mathrm{GeV}^2)$ measurements at JLab[31,32] discussed in Sec. 6. In Fig. 3 the ratio (5) is presented as a function of spectator nucleon angle, θ_{nq}, for different values of recoil neutron (or missing) momenta. All data are at sufficiently large Q^2 kinematics for which one expects the onset of eikonal regime. Figure 3(a) which presents the Hall A data,[32] shows a clear diffractive pattern of the FSI in which at small recoil momenta ($p_r < 300\,\mathrm{MeV}/c$) the ratio, R, is depleted due to screening effects ($R < 1$) while at larger momenta ($p_r > 300\,\mathrm{MeV}/c$) one observes a diffractive FSI peak with $R > 1$. The same feature are visible in Fig. 3(b) where CLAS/Hall B data[31] are presented. In this case, despite the large range of integrations of recoil neutron momenta one still can see distinctive diffractive pattern of FSI.

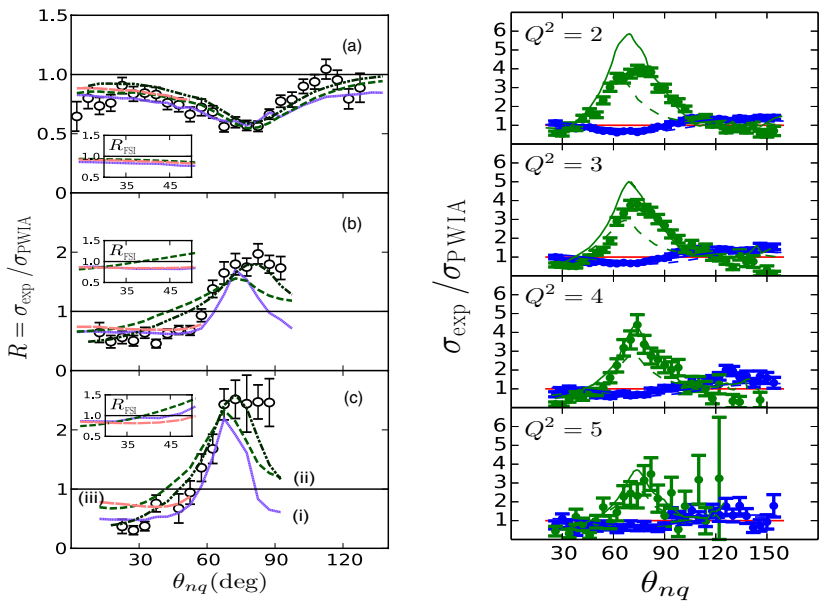

Fig. 3. (Color online) The ratio $R(\theta_{nq})$ of Eq. (5). (a) Hall A data (a) $p_m = 0.2$ GeV/c, (b) $p_m = 0.4$ GeV/c and (c) $p_m = 0.5$ GeV/c (See panels of Fig. 3(a)). Solid (purple) curves (i) prediction of Refs. 22, 24 and 33 using the charge-dependent Bonn nucleon–nucleon (CD-Bonn) potential, short-dashed (green) curves; (ii) prediction of Ref. 34, dashed–double-dot curves prediction of Ref. 34 including MEC and IC effects, and long-dashed (orange) lines and (iii) prediction of Ref. 35. Insets: R for the range of $35° \leq \theta_{nq} \leq 45°$. (b) CLAS/Hall B data. The data points that exhibit rescattering peaks at transverse kinematics correspond to $400\,\mathrm{Mev}/c \leq p_m \leq 600\,\mathrm{MeV}/c$, and the others without rescattering peaks correspond to $200\,\mathrm{Mev}/c \leq p_m \leq 300\,\mathrm{MeV}/c$ (see panels of Fig. 3(b)). Solid curves are prediction of Ref. 34 and dashed ones are prediction of Ref. 24.

The other important feature of Fig. 3 is the observation of the above discussed cancellations of the FSI in forward ∼40° and backward ∼120° directions of recoil neutron production. These cancelations allow one to probe the "genuine" deuteron momentum distribution beyond 300 MeV/c. In further discussions we will concentrate only on the forward direction of the recoil neutron production. The reason is that the kinematics of the backward production of a recoil neutron is close to the inelastic threshold of $\gamma^* p$ and as a result, for not very large Q^2 ($2\,\text{GeV}^2 \leq Q^2 \leq 4\,\text{GeV}^2$) there is a considerable contribution from processes with intermediate Δ resonance production (Fig. 1(i)).

8. First Measurements of the Deuteron Momentum Distribution Beyond 300 MeV/C

The discussions of the Secs. 4 and 7 allow us to make two main conclusions: (i) providing kinematic constraints of Eq. (4) allows us to suppress all but FSI contributions which obscure the scattering from the high momentum component of the deuteron; (ii) high energy eikonal kinematics create a unique condition for the cancelation of the FSI contribution in the forward, $\theta_{nq} \leq 40°$, direction of spectator nucleon production.

As it was discussed in Secs. 6 and 7 the first two high Q^2 experiments performed recently at JLab[31,32] satisfy these conditions and their measured spectator nucleon angular distributions clearly demonstrate the onset of the eikonal regime for FSI, Fig. 3. Thus, one expects that the momentum dependence of the cross-section of the reaction (1) measured at $\theta_{nq} \leq 40°$ directions and $p_r > 300\,\text{MeV}/c$ momenta

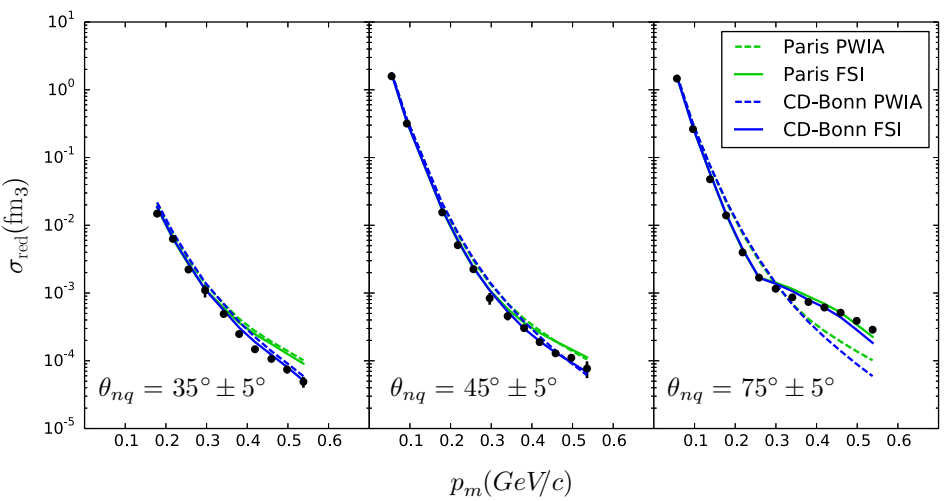

Fig. 4. (Color online) The experimental reduced cross sections (momentum distributions) for three values of the recoil angle θ_{nq}. The solid lines indicate calculations[24] including FSI and the dashed ones are PWIA calculations.

will be related to the genuine high momentum component of the deuteron wave function.

Such a dependence was extracted from the experimental data of Ref. 32 in which the reduced cross-section (6) was measured for fixed $Q^2 = 3.5$ GeV^2 for recoil nucleon momenta up to 550 MeV/c. The ability of this experiment to separate narrow θ_{nq} bins in the momentum distribution was important for separating regions with different degrees of FSI contribution.

As an illustration in Fig. 4 the missing momentum dependence for fixed recoil (neutron) angles $\theta_{nq} = 35^\circ$, 45° and 75° degrees are shown for the reduced cross-section defined in Eq. (6). For comparison, theoretical calculations of Ref. 24 with and without FSI are also shown. For the large recoil angle, ($\theta_{nq} = 75^\circ$) corresponding to an electron kinematics of $x_B \approx 1$ FSI dominates for missing momenta above 0.3 GeV/c and the sensitivity to the choice of the deuteron wave function is greatly reduced. In fact the momentum dependence in this case strongly resembles that of the low and intermediate energies (Fig. 2).

The momentum dependence of the reduced cross section at large p_m qualitatively changes at small angles. As Fig. 4 shows for $\theta_{nq} = 35^\circ$ and 45° FSI contributes significantly less and the reduced cross-section is much more sensitive to the details of the high momentum distribution, allowing us for the first time to discriminate between different models of the deuteron wave function.

9. The First Extraction of the Light-Cone Momentum Distribution of the Deuteron

The availability of high Q^2 data on exclusive electrodisintegration of the deuteron provides, for the first time, the possibility to extract directly the light-cone momentum distribution of the deuteron $\rho_d(\alpha)$, where α represents light-cone momentum fraction of the struck nucleon normalized in such way that the total light-cone momentum fraction of the deuteron is two. The α variable satisfies the condition: $0 \leq \alpha \leq 2$ and from the momentum–energy conservation it follows that $\alpha + \alpha_r = 2$, where α_r is the momentum fraction of the recoil nucleon.

The function $\rho_d(\alpha)$ plays an essential role in studies of inclusive and semiinclusive deep inelastic scattering (DIS) off the deuteron which are used for studies of the partonic structure of the neutron. For example, for inclusive scattering, in the high Q^2 limit, the experimental DIS structure function of the deuteron F_{2d} can be expressed through the bound nucleon structure functions $F_{2N}^{\rm bound}$ as follows:

$$F_{2d}(x_{Bj}, Q^2) = \int_{x_{Bj}}^{2} F_{2p}^{\rm bound}\left(\frac{x_{Bj}}{\alpha}, Q^2\right) \rho_d(\alpha) \frac{d\alpha}{\alpha} + \int_{x_{Bj}}^{2} F_{2n}^{\rm bound}\left(\frac{x_{Bj}}{\alpha}, Q^2\right) \rho_d(\alpha) \frac{d\alpha}{\alpha}, \tag{16}$$

which indicates that the knowledge of the structure function of the bound proton $\tilde{F}_{2p}^{\rm bound}$ as well as $\rho_d(\alpha)$ is necessary for the extraction of $F_{2n}^{\rm bound}(x_{Bj})$ which is

largely unknown at $x_{Bj} > 0.7$. Here the function $\rho_d(\alpha)$ satisfied two sum rules:

$$\int_0^2 \rho_d(\alpha)\frac{d\alpha}{\alpha} = 1 \quad \text{and} \quad \int_0^2 \rho_d(\alpha)\alpha\frac{d\alpha}{\alpha} = 1, \tag{17}$$

where the first follows from the requirement of the conservation of the baryonic number and the second represents the momentum sum rule (see e.g., Ref. 49).

It is worth noting that $\frac{\rho_d(\alpha)}{\alpha}$ is analogous to the partonic distribution function $f_i(x)$ but for nucleonic degrees of freedom (for details see e.g., Ref. 50). And similar to partonic distribution functions one can introduce the unintegrated function $\rho_d(\alpha, p_t)$ such that

$$\rho_d(\alpha) = \int \rho_d(\alpha, p_t)d^2p_t. \tag{18}$$

The unintegrated density function $\rho_d(\alpha, p_t)$ can be expressed through the light-cone wave function of the deuteron as follows:

$$\rho(\alpha, p_t) = \frac{|\psi_d^{\rm LC}(\alpha, p_t)|^2}{2-\alpha}. \tag{19}$$

On the fundamental level to calculate the light-cone wave function of the deuteron one needs to identify the NN interaction potentials on the light front and solve the Weinberg-type equations[51] for two-body bound systems. Such a program is tremendously difficult (see e.g., Ref. 52) and in reality different theoretical approximations are made to model the light-cone wave function of the deuteron (see e.g., Ref. 49).

One concludes from the above discussion that the possibility of an experimental extraction of the ρ_d function is important from both theoretical and experimental point of views. For theory, it will make it possible to check different approaches in calculating the deuteron wave function within light-cone dynamics and for experiment, the extracted distribution can be used as an input in studies of DIS processes involving deuteron.

The idea that one can extract the $\rho_d(\alpha)$ from the reaction (1) follows from the theoretical observation[24] that in the high energy limit FSI processes (Fig. 1(c)) do not modify the initial light-cone momentum fraction of the struck nucleon α. This can be seen analytically by observing that the FSI diagram of Eq. (7) on the light cone can be represented as follows[24]:

$$A_1^\mu = \sqrt{2(2\pi)^3 2m_N}\int \frac{d\alpha' d2p'_{it}}{2\alpha'(2\pi)^3}\frac{\sqrt{s(s-4m_N^2)}}{2m_N q}\frac{f_{pn}(p'_{it}-p_{it})}{\alpha'-\alpha-\frac{Q^2}{2q^2}\frac{E_n-m_N}{m_N}+i\varepsilon}$$
$$\times j_N^\mu(\alpha', p'_{it}+q, \alpha_i, p'_{it})\psi_d^{\rm LC}(\alpha', p'_{it}), \tag{20}$$

from which one observes that in the limit of $\frac{Q^2}{2q^2}\frac{E_n-m_N}{m_N} \ll 1$ the pole value in the integrand corresponds to $\alpha = \alpha'$ which indicates that the FSI does not change the light-cone momentum fraction, α of the initial nucleon.

The above result qualitatively means that the FSI will redistribute the scattering strength only in the transverse, p_t direction, therefore if one extracts the p_t integrated light-cone density function $\rho_d(\alpha)$ from the experiment, it will be minimally modified due to FSI.

Recently, the first attempt has been made to extract the $\rho(\alpha)$ function from the $Q^2 = 3.5\,\mathrm{Gev}^2$ data measured at Hall A/JLab. For this, the data set described in Sec. 6, have been analyzed in terms of the light cone variables α, p_t. On an event-by-event basis the recoiling neutron momentum fraction α_n and the transverse momentum, p_{tn}, (with respect to the $\mathbf{q}$) have been calculated. The initial light-cone momentum fraction and the transverse momentum of the interacting nucleon (proton) was calculated using the relation: $\alpha = 2 - \alpha_n$ and $p_t = -p_{tn}$. Then in a completely analogous way as the standard $d(e, e'p)n$ analysis, the experimental yields for the different kinematic settings have been normalized, radiatively corrected and for each α, p_t bin a differential cross-section has been determined. The various kinematic settings have then been combined by averaging overlapping bins.

The extraction of $\rho(\alpha, p_t)$ was made based on the theoretical framework of light-cone PWIA according to which:

$$\frac{d\sigma}{dEe'd\Omega_e d\Omega_s} = K\sigma_{eN}^{\mathrm{LC}}(\alpha, p_t)\rho(\alpha, p_t), \tag{21}$$

where $\alpha = 2 - \alpha_n$, $\alpha_n = \frac{E_n - p_{n,z}}{M_d/2}$ and k is a kinematic factor.

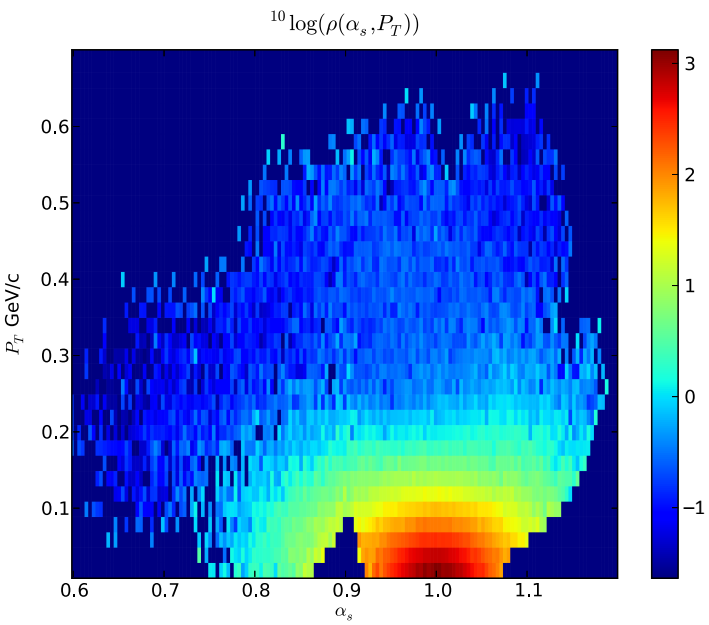

Fig. 5. (Color online) The experimental $\rho(\alpha, p_t)$ distribution.

To extract the ρ function the evaluated experimental cross sections have been divided by the corresponding light-cone electron–proton (e–p) cross-section, $\sigma_{eN}^{\rm LC}(\alpha, p_t)$, and the kinematic factor K. This, according to Eq. (21) allowed one to obtain the 'experimental' distribution $\rho(\alpha, p_t)$ presented in Fig. 5.

The data presented in Fig. 5 makes it possible to study the transverse momentum, p_t distribution for constant α or vice versa. Especially interesting is the integration of $\rho(\alpha, p_t)$ over p_t for which one can check the sum rules of Eq. (17). The satisfaction of these sum rules will be indicative of the cancelation of the FSI In the $\rho(\alpha)$ distribution.

To perform the p_t integration and extract the $\rho(\alpha)$ we fitted model distributions to the data for slices of constant p_t, which was necessary as the kinematic coverage in the available data set is not complete. Using the fitted α distributions we could interpolate between bins where no data exist and use these in the integration over p_t. This procedure then leads to the experimental $\rho(\alpha)$ distribution, shown in Fig. 6. In the same figure the results of the baryonic and momentum sum rules are presented which indicate a reasonable agreement with Eq. (17). The agreement with both sum rules is the strongest indication that FSI redistributes the cross-section in the transverse momentum space and as a result the integrated $\rho_d(\alpha)$ distribution represents the unaltered light-cone momentum fraction distribution of the nucleon in the deuteron.

Our conclusion is that the first analysis demonstrates the feasibility of an experimental extraction of the integrated light-cone momentum distribution of the deuteron and new data with wider kinematical coverage will allow to increase significantly the accuracy of such an extraction.

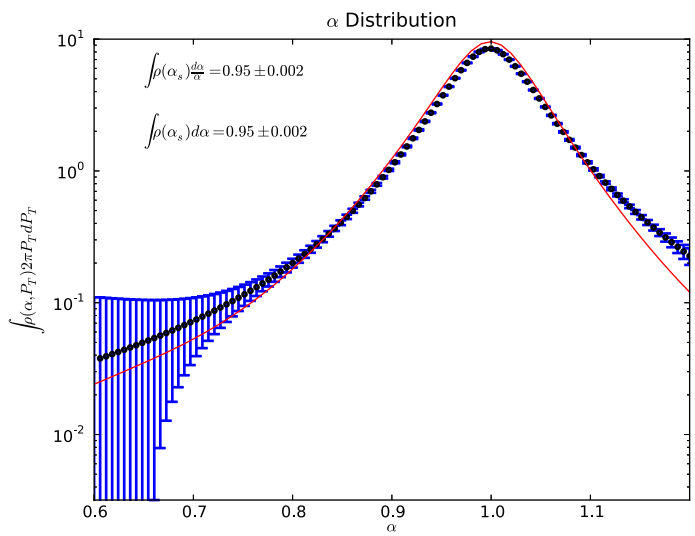

Fig. 6. (Color online) The experimental $\rho(\alpha)$ distribution, integrated over p_t.

10. Summary and Outlook for Future Studies of the Deuteron

In this paper, we presented the current status of studies of the deuteron at large internal momenta and demonstrated that the possibility of performing exclusive $d(e, e'N)N$ experiments at large momentum and energy transfers satisfying the kinematical conditions of Eq. (4), opens up a window to probing the deuteron structure at small distances.

As we discussed, the attempts to determine the deuteron momentum distribution for missing momenta above $300\,\mathrm{MeV}/c$ at low momentum transfer experiments suffered from the large contributions from FSI, MEC and IC effects which are dominated by the long-range structure of the deuteron. We then demonstrated that by increasing the momentum and energy transfers above the GeV limit allows one to suppress MEC and IC contributions while for FSI the eikonal regime is established. The eikonal regime is characterized by a very anisotropic angular distribution of the recoil nucleon production and it makes it possible to identify kinematical regions where FSI are mostly cancelled.

The first high energy data confirm the angular distribution characteristic of FSI in the eikonal regime. Then, using the high precision $Q^2 = 3.5\ \mathrm{GeV}^2$ data at the kinematics were one expects FSI cancelation to occur, we probed the deuteron in a missing momentum region of 300–$500\,\mathrm{MeV}/c$ without large contributions of FSI, MEC or IC.

Another new venue in probing the deuteron at small distances and high momentum transfers is the use of the approximate conservation of the light-cone momentum fraction α in the high energy limit to extract the light-cone momentum distribution function $\rho(\alpha)$ which is minimally altered by FSI.

The above concepts can be extended to the deuteron studies at the completely unexplored internal momentum range of $\sim 1\,\mathrm{GeV}/c$. Such studies are fascinating since for the first time one will have an opportunity to probe a nuclear bound state at distances relevant to the NN core.

As Fig. 7 demonstrates, at large Q^2 it is still possible to identify the kinematic window of minimal FSI effects for missing momenta of the reaction up to $1\,\mathrm{GeV}/c$. This gives a possibility to extend the studies of the deuteron beyond $550\,\mathrm{MeV}/c$. A first such attempt will be made in the approved experiment of Ref. 53 which will be carried out at the JLab with the electron beam upgraded to the 11 GeV. This experiment will reach a momentum transfer of $Q^2 = 4.25\,(\mathrm{Gev/c})^2$ with recoil neutron angle covering the forward, 35–40°, region were one expects reduced FSI (Fig. 7).

The large value of the Q^2 will be essential for satisfying the condition of Eq. (4) which is necessary for identifying the $1\,\mathrm{GeV}/c$ neutron as a spectator (preexisting) nucleon in the deuteron, thereby providing the condition of probing NN distances relevant to $1\,\mathrm{GeV}/c$ relative momentum in the deuteron.

In addition, the possibility of the measurement of the angular distribution for $p_m > 550\,\mathrm{MeV}/c$ will allow the extension of the range of α at which the light-cone

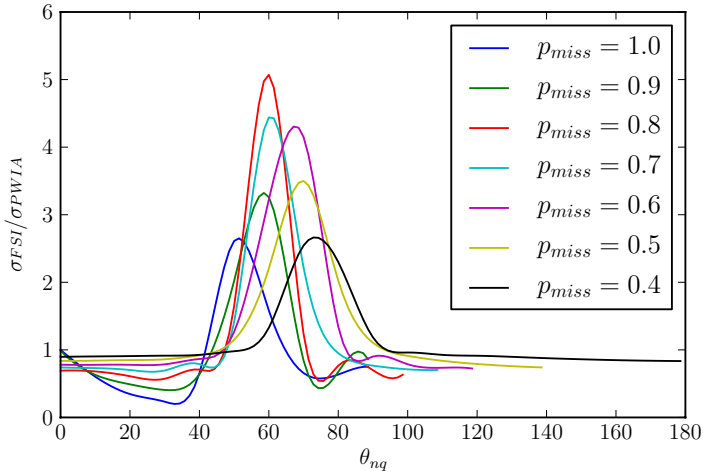

Fig. 7. (Color online) Ratios of the calculated cross sections including FSI effects $\sigma_{\rm FSI}$ to that of the PWIA at different values of missing momenta as a function of the neutron recoil angle.

momentum distribution of the deuteron, $\rho(\alpha)$ can be extracted. The study of the deuteron structure on the light-cone has just started. A good kinematic coverage is required to reduce the model dependence of the determination of $\rho(\alpha)$. If necessary, new data could be obtained using new detector systems which have large acceptances allowing high luminosity beams. Such a situation will allow the measurement of very small coincidence cross sections of reaction (1). The next stage of such studies will be the extension of the reaction to the case of a polarized electron beam and polarized deuteron target. The study of the deuteron light-cone wave function using polarization degrees of freedom is currently being studied.

Finally, the deuteron structure can be probed in deep inelastic hard processes such as hard breakup of the deuteron[54,55] and deep inelastic electroproductions of photons and vector mesons aimed at studies of the generalized partonic distributions in the deuteron (see e.g., Refs. 56 and 57).

All the above mentioned studies will be an important step in designing a new generation of experiments with the further goal of probing even shorter distances relevant to the non-nucleonic as well as quark-gluon content of the deuteron.

Acknowledgments

The authors are thankful to Dr. C. Ciofi degli Atti, Dr. L. Frankfurt, Dr. J. M. Laget, Dr. S. Jeschonnek, Dr. M. Jones, Dr. W. Van Orden, Dr. G. Miller, Dr. M. Strikman, Dr. E. Voutier for helpful comments and discussions. This work is supported by US DOE grants under contract DE-FG02-01ER41172 and DE-FG02-99ER41065.

References

1. D. O'Leary, *Nat. Chem.* **4** (2012) 236.
2. J. Hockert, D. Riska, M. Gari and A. Huffman, *Nucl. Phys. A* **217** (1973) 14.
3. W. Fabian and H. Arenhovel, *Nucl. Phys. A* **258** (1976) 461.
4. H. Weber and H. Arenhovel, *Phys. Rept.* **36** (1978) 277.
5. S. J. Brodsky and B. Chertok, *Phys. Rev. Lett.* **37** (1976) 269.
6. M. Harvey, *Nucl. Phys. A* **352** (1981) 326.
7. C.-R. Ji and S. J. Brodsky, *Phys. Rev. D* **34** (1986) 1460.
8. E. Piasetzky, M. Sargsian, L. Frankfurt, M. Strikman and J. Watson, *Phys. Rev. Lett.* **97** (2006) 162504, arXiv:nucl-th/0604012.
9. M. M. Sargsian, *Phys. Rev. C* **89** (2014) 034305, arXiv:1210.3280 [nucl-th].
10. O. Hen *et al.*, *Science* **346** (2014) 614, arXiv:1412.0138 [nucl-ex].
11. O. Hen, L. Weinstein, E. Piasetzky, G. Miller and M. Sargsian, arXiv:1407.8175 [nucl-ex].
12. R. A. Gilman and F. Gross, *J. Phys. G* **28** (2002) R37, arXiv:nucl-th/0111015.
13. J. Arrington, D. Higinbotham, G. Rosner and M. Sargsian, *Prog. Part. Nucl. Phys.* **67** (2012) 898, arXiv:1104.1196 [nucl-ex].
14. M. Croissiaux, *Phys. Rev.* **127** (1962) 613.
15. P. Bounin and M. Croissiaux, *Nucl. Phys* **70** (1965) 401.
16. Y. Antufev, V. Agranovich, V. Kuzmenko and P. Sorokin, *Yad. Fiz.* **22** (1975) 236.
17. Y. Antufev, V. Agranovich, V. Kuzmenko and P. Sorokin, *Pis'ma Zh. Eksp. Teor. Fiz.* **19** (1974) 657.
18. A. Bussiere *et al.*, *Nucl. Phys. A* **365** (1981) 349.
19. S. Turck-Chieze *et al.*, *Phys. Lett. B* **142** (1984) 145.
20. L. Frankfurt, M. Sargsian and M. Strikman, *Int. J. Mod. Phys. A* **23** (2008) 2991. arXiv:0806.4412 [nucl-th].
21. L. Frankfurt and M. Strikman, *Phys. Rept.* **160** (1988) 235.
22. M. M. Sargsian, *Int. J. Mod. Phys. E* **10** (2001) 405. arXiv:nucl-th/0110053.
23. M. Sargsian *et al.*, *J. Phys. G* **29** (2003) RI, arXiv:nucl-th/0210025.
24. M. M. Sargsian, *Phys. Rev. C* **82** (2010) 014612, arXiv:0910.2016 [nucl-th].
25. P. Stoler, *Phys. Rep.* **226** (1993) 103.
26. CLAS Collab. (M. Ungaro *et al.*), *Phys. Rev. Lett.* **97** (2006) 112003, arXiv:hep-ex/0606042.
27. L. Durand, *Phys. Rev.* **115** (1959) 1020.
28. H. Arenhovel, private communcation (2013).
29. K. Blomqvist *et al.*, *Phys. Lett. B* **424** (1998) 33.
30. W. Boeglin *et al.*, *Phys. Rev. C* **78** (2008) 054001, arXiv:0804.3722 [nucl-ex].
31. CLAS Collab. (K. Egiyan *et al.*), *Phys. Rev. Lett.* **98** (2007) 262502, arXiv:nucl-ex/0701013.
32. Hall A Collab. (W. Boeglin *et al.*), *Phys. Rev. Lett.* **107** (2011) 262501, arXiv:1106.0275 [nucl-ex].
33. L. Frankfurt, M. Sargsian and M. Strikman, *Phys. Rev. C* **56** (1997) 1124, arXiv:nucl-th/9603018.
34. J. Laget, *Phys. Lett. B* **609** (2005) 49, arXiv:nucl-th/0407072.
35. S. Jeschonnek and J. Van Orden, *Phys. Rev. C* **78** (2008) 014007, arXiv:0805.3115 [nucl-th].
36. I. Sick and D. Trautmann, *Phys. Lett. B* **375** (1996) 1620.
37. R. B. Wiringa, V. Stoks and R. Schiavilla, *Phys. Rev. C* **51** (1995) 38, arXiv:nucl-th/9408016.

38. L. Frankfurt, W. Greenberg, G. Miller, M. Sargsian and M. Strikman, *Z. Phys. A* **352** (1995) 97, arXiv:nucl-th/9501009.
39. A. Bianconi, S. Jeschonnek, N. N. Nikolaev and B. Zakharov, *Phys. Lett. B* **343** (1995) 13, arXiv:nucl-th/9409014.
40. L. Frankfurt, E. Piasetzky, M. Ssrgsian and M. Strikman, *Phys. Rev. C* **56** (1997) 2752, arXiv:hep-ph/9607395.
41. J.-M. Laget, in Workshop Phys. High-Energy Real Photons, 1998 (Grenoble, France, 1998).
42. S. Jeschonnek, *Phys. Rev. C* **63** (2001) 034609, arXiv:nucl-th/0009086.
43. C. C. degli Atti, L. Kaptari and D. Treleani, *Phys. Rev. C* **63** (2001) 044601, arXiv:nucl-th/0005027.
44. C. C. degli Atti and L. Kaptari, *Phys. Rev. C* **71** (2005) 024005, arXiv:nucl-th/0407024.
45. M. Sargsian, T. Abrahamyan, M. Strikman and L. Frankfurt, *Phys. Rev. C* **71** (2005a) 044614, arXiv:nucl-th/0406020.
46. M. Sargsian, T. Abrahamyan, M. Strikman and L. Frankfurt, *Phys. Rev. C* **71** (2005b) 044615, arXiv:nucl-th/0501018.
47. W. Cosyn and M. Sargsian, *Phys. Rev. C* **84** (2011) 014601, arXiv:1012.0293 [nucl-th].
48. W. P. Ford and J. van Orden, *Phys. Rev. C* **88** (2013) 054004, arXiv:1306.6925 [nucl-th].
49. L. Frankfurt and M. Strikman, *Phys. Rep.* **76** (1981) 215.
50. A. J. Freese, M. M. Sargsian and M. I. Strikman, arXiv:1411.6605 [hep-ph].
51. S. Weinberg, *Phys. Rev.* **150** (1966) 1313.
52. J. R. Cooke and G. A. Miller, *Phys. Rev. C* **66** (2002) 034002, arXiv:nucl-th/0112037.
53. W. Boeglin *et al.*, arXiv:1410.6770[nucl-ex].
54. L. L. Frankfurt, G. A. Miller, M. M. Sargsian and M. I. Strikman, *Phys. Rev. Lett.* **84** (2000) 3045, arXiv:hep-ph/9904222.
55. C. G. Granados and M. M. Sargsian, *Phys. Rev. C* **83** (2011) 054606, arXiv:1007.4705 [hep-ph].
56. F. Cano and B. Pire, *Eur. Phys. J. A* **19** (2004) 423, arXiv:hep-ph/0307231.
57. E. R. Berger, F. Cano, M. Diehl and B. Pire, *Phys. Rev. Lett.* **87** (2001) 142302, arXiv:hep-ph/0106192.